Calculation of images of oriented C_{60} molecules using molecular orbital theory

Ian D. Hands, Janette L. Dunn,* and Colin A. Bates
School of Physics and Astronomy, University of Nottingham, Nottingham NG7 2RD, United Kingdom
(Received 22 February 2010; revised manuscript received 4 May 2010; published 26 May 2010)

Using Hückel molecular-orbital theory, images are created to represent the electron distributions expected for a C_{60} molecule adsorbed on a substrate. Three different orientations of the C_{60} molecule on the substrate are considered. The effect of the interaction of the molecule with the substrate is treated purely from the basis of symmetry using group theoretical methods. The resulting electron distributions are then used to generate idealized images which represent how the molecule may appear when observed in a scanning tunneling microscope (STM) experiment. Comparison is made with STM images appearing in the literature. It is found that the more complicated *ab initio* methods usually employed to simulate STM images are not required in order to match observed results. Furthermore, we find that an unequivocal identification of the orbitals responsible for a given STM image cannot be made from analysis of the STM image alone.

DOI: 10.1103/PhysRevB.81.205440 PACS number(s): 61.48.−c, 68.37.Ef, 31.15.ae

I. INTRODUCTION

The C_{60} molecule is an ideal candidate for study via scanning tunneling microscopy (STM) as the molecule's size makes it readily visible. Furthermore, high-resolution STM is able to resolve intramolecular features which appear to confirm the icosahedral character of the molecule. However, in order to image C_{60} molecules, it is necessary for them to lie on a solid surface, which in general will induce interactions with the surface. In some papers, attempts have been made to decouple the molecules from a substrate. For example, Frederiksen *et al.*[1] examined transport through single C_{60} molecules decoupled from a surface by a template of organic molecules and Silien *et al.*[2] reduced interactions with a Cu(111) surface by precoating the substrate with a layer of potassium. However, in the majority of papers, the C_{60} molecules are adsorbed directly on to a substrate. This will necessarily remove the inversion symmetry required to maintain the icosahedral symmetry of C_{60} and results in a reduction in the degeneracy of the frontier molecular orbitals that are normally imaged. This was seen in Silien *et al.*,[2] where the lowest unoccupied molecular orbital (LUMO) of C_{60} molecules on a Cu(111) surface is split into two states while only a single electronic state is observed when the Cu(111) is precoated in potassium.

As observed STM images are affected by interactions with a substrate, these interactions cannot be ignored. In this paper, we will use group theoretical methods to probe the role of this interaction. The images observed will, in general, depend on both the orientation of the C_{60} molecule and the symmetry of the adsorption site. However, there is found to be only a weak dependence on the adsorption site.[3] We will therefore only consider the effect of different orientations here. Care must be taken when deducing the orientation of C_{60} molecules from STM images as they show the electron density and not the position of the carbon atoms directly. However, as the electron density is highest along the bonds, the appearance of pentagons or hexagons in the STM images is a reasonable indicator that a pentagon or hexagon is uppermost, and hence also prone to the surface. This is particularly true of observed pentagons[4] as no other orientation is likely to result in a pentagonal image.

On Au(111), Lu *et al.*[5] observe isolated molecules in five different orientations, namely, with a hexagon, pentagon, single bond, double bond, and edge atom prone to the surface. Most other papers look at a monolayer (or more) of C_{60} molecules rather than isolated molecules. A hexagonal face is found to be facing the substrate by Li *et al.*[6] on an Ag(111) surface and Hashizume *et al.*[7] on a Cu(111) surface. Likewise, Silien *et al.*[2] report that the majority of molecules on Cu(111) bond with a hexagon down. However, Silien *et al.*[2] find that a small portion of molecules on Cu(111) bond with a pentagon down. On an Au(111) surface, Altman and Colton[8] observe images of the LUMO on C_{60} that have fivefold symmetry which they attribute to a pentagon prone to the surface while Wachowiak *et al.*[9] has images consistent with a hexagon down for A_3C_{60} and with a double bond down for A_4C_{60}. On a Si(111) 7×7 surface, it appears that C_{60} is oriented such that either a single bond or an edge atom faces the surface.[3] Similarly, on a Si(100) 2×1 surface there is an indication that C_{60} exhibits a twofold symmetry,[10] which would be indicative of either a single or a double bond facing the surface.[7]

While intermolecular interactions between C_{60} molecules in a monolayer will have some effect on the observed images, these will be neglected in this paper. We will also ignore other features such as the effects of charge transfer between C_{60} and the surface, and of molecular distortions due to geometric effects or Jahn-Teller (JT) interactions. We will discuss these points further at the end of this paper.

As a range of orientations of C_{60} have been proposed to explain the observed STM images, we will consider the three cases of a pentagonal face, hexagonal face, and (carbon-carbon) double bond prone to the surface. We will assume that the interaction with the surface is sufficiently weak that it causes a simple splitting of the relevant molecule orbitals: viz, the highest occupied (HOMO), LUMO, and next-lowest unoccupied (LUMO+1) orbitals. However, the splitting is assumed to be sufficiently large that each split component can be imaged without interference from adjacent orbitals.

For each orientation, basis vectors are generated for the irreducible representations (irreps.) of interest and combinations of orbitals created that possess identical transformation properties. Simulations of images that could be obtained

when a C_{60} molecule is imaged are then obtained using Hückel molecular orbital (HMO) theory on these combinations of orbitals. Although the simplifying assumptions mentioned in the last two paragraphs are used to produce the images, the results provide an insight into the images expected to be observed in actual STM experiments. Comparisons made with published results in the literature will show that it is not necessary to use the *ab initio* methods that are more usually used to produce simulations of STM images.

II. THEORY

We will first describe the HMOs used and discuss how we will model the surface interaction. We will then give details of how our method can be applied to the case of C_{60} molecules with a pentagonal face prone to the surface. We then give the results for when the same method is applied to C_{60} molecules in the hexagon and double bond-prone orientations.

A. Molecular orbitals

The HMOs will be assumed to be created from the 60 p orbitals located at the 60 carbon atoms in C_{60}. The linear combinations required to form all 60 HMOs have been formulated in a concise manner by Deng and Yang,[11] and we use a modified version of their results here. As their work uses a coordinate system in which C_{60} is oriented so that a C_5 axis coincides with the z axis, they can be applied most readily to a pentagon-prone molecule. This is why we will deal with this orientation first. It should be noted that Deng and Yang[11] tabulate expressions for the HMOs that apply to the case where single and double carbon-carbon bonds are equivalent, that is, their respective resonance integrals β_s and β_d are taken to be equal. In the current work, we adopt a more realistic picture in which $\beta_s \neq \beta_d$. In the literature, this is often referred to as bond "alternation". In an earlier work,[12] we used a parameter $\tau=\beta_d/\beta_s$ to account for this inequality. Ref. 11 used an alternative parameter $\alpha=-\beta_s$, which requires that $\beta_d=\alpha-2$. This in turn implies that the two treatments are related by $\alpha=2(1+\tau)^{-1}$. Consequently, the simple equal-bond picture corresponds to the case $\alpha=\tau=1$. In Ref. 12, the value $\tau=1.433$ was derived in order to explain the experimentally observed bond alternation of $r(\mathrm{C{=}C})=1.391$ Å and $r(\mathrm{C{-}C})=1.455$ Å. This, in turn, implies that $\alpha=0.8220$ which is the value that we adopt from this point on.

Using the modified results of Deng and Yang,[11] we can generate the necessary coefficients to construct the required combination of molecular orbitals. In order to produce an image, we assume that the wave functions decay as e^{-kr}, where, for hydrogenlike atoms, $k=Z_{\mathrm{eff}}/2a_0$, with Z_{eff} the effective nuclear charge and a_0 the Bohr radius. Furthermore, we take the effective nuclear charge to be 3.14, as determined by Clementi and Raimondi,[13] corresponding to $k \approx 3$ Å^{-1}.

B. Surface interactions

For isolated C_{60} molecules, the LUMO and LUMO+1 are triply degenerate states of symmetry T_{1u} and T_{1g}, respectively, and the HOMO is a fivefold degenerate state of H_u symmetry. An STM experiment on such a molecule would, therefore, be expected to visualize the three degenerate sets of orbitals at three different biases. However, as mentioned above, this picture will change in the presence of a host substrate due to interactions with the substrate. The individual members of each irrep. will interact with the surface to differing degrees leading to a reduction in the degeneracy. Different components of the HMOs will have different energies and will hence be imaged at different biases in STM experiments.

Formally, there are 17 two-dimensional space groups arising from five Bravais nets associated with translation over a surface.[14] A C_{60} molecule adsorbed onto a surface will therefore be subject to a local symmetry belonging to one of ten possible site symmetries: C_{6v}, C_6, C_{4v}, C_4, C_{3v}, C_3, C_{2v}, C_2, C_s, and C_1. The actual symmetry of the registration site depends on the surface used. For example, molecules on a Cu(111) surface are found to occupy a threefold site.[2,7] Sites with a possible sixfold symmetry are not observed experimentally.[7] Single C_{60} molecules on a Pt(111) surface are found to reside in a fourfold site.[15] In this paper, we will consider the case where C_{60} is subject to a local field of C_{6v} symmetry, as this is the highest of the allowed symmetries. However, extension to sites of lower symmetry is readily accomplished if required. Also, as mentioned above, the exact symmetry of the local field is not as important as the orientation of the C_{60} molecule.[3] The biggest effect of the field due to the substrate on the C_{60} molecules is to lift degeneracies in the molecular orbitals. None of the site groups support irreps. with a degeneracy greater than two so all of the symmetries will lift some of the degeneracies. This will be discussed again in Sec. III.

In order to determine the effect of the reduction in symmetry due to surface interactions, we will use a method reminiscent of the group theoretical technique used by Bhagavantam and Suryanarayana[16] to investigate the effect of symmetry on the tensorial properties of physical phenomena. However, before we can proceed, we need to specify an appropriate coordinate system and obtain basis functions for the HMOs in that system. As the direction perpendicular to the surface is likely to be associated with a different symmetry to the directions in the plane of the surface, it seems natural to define a Cartesian z axis to be perpendicular to the surface. This means that we will have a different molecular z axis for different orientations of the C_{60} molecule on the surface. For example, when a pentagonal face is prone to the surface, the z axis will pass through the center of the pentagon, which coincides with a C_5 symmetry axis. When a hexagonal face is prone to the surface, the z axis will coincide with a C_3 symmetry axis.

A consequence of our choice of axes is that we will need to determine different basis functions for the different orientations. However, we find that this is the easiest way to determine the effect of the surface interaction. An alternative method would be to use the same molecular basis for all orientations and consider the surface to be in different directions for different orientations. However, the direction perpendicular to the surface would then, in general, be a combination of x, y, and z. The HMO in this direction would also

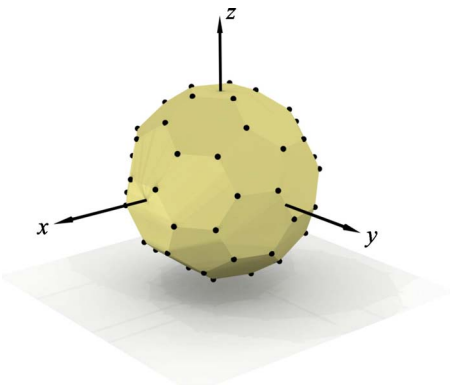

FIG. 1. (Color online) Definition of Cartesian axes and positions of atoms for a C_{60} molecule with a pentagon prone to a surface.

be a combination of x, y, and z. It would be necessary to determine these combinations in order to determine the effect of the surface interaction, which is not a trivial task.

C. Pentagon-prone C_{60} molecules

For a pentagon-prone molecule, the Cartesian z axis perpendicular to the surface coincides with a C_5 symmetry axis. We define a y axis to be collinear with a C_2 axis, as shown in Fig. 1. Such a configuration matches that used in Ref. 11 and so expressions for the HMOs of C_{60} for this arrangement are already readily available.

In order to investigate the transformation properties of the HMOs, we look for basis functions that transform in the same way. This is accomplished using the method outlined by Chancey and O'Brien.[17] The technique involves diagonalizing an icosahedral crystal field of the form

$$V_{\text{icos}} = 231z^6 - 315r^2z^4 + 105r^4z^2 - 5r^6 + 42xz(x^4 - 10x^2y^2 + 5y^4) \quad (1)$$

using angular momentum states. The potential V_{icos}, depicted in Fig. 2, is oriented in such a way that it matches our pentagon-prone configuration. Thus, there is a one-to-one correspondence between the basis functions in this configuration and the HMOs derived by Deng and Yang.

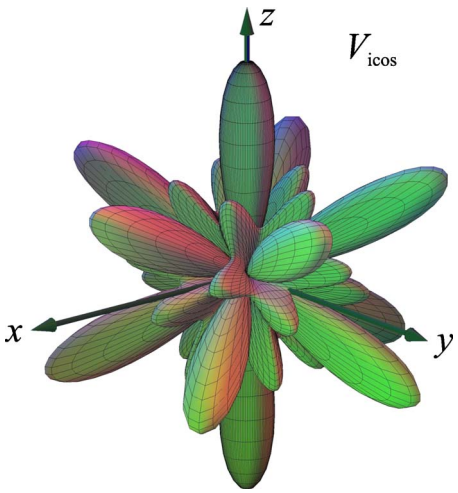

FIG. 2. (Color online) The potential used to generate basis vectors for a pentagonal-prone C_{60} molecule.

The resulting basis functions for the HOMO, LUMO, and LUMO+1 orbitals of C_{60} are collected together in Table I. They are labeled according to their transformation properties, so, for example, the irrep. labeled H^p_{uyz} transforms as the product yz in I_h symmetry. The superscript "p" signifies that the molecule is pentagon prone to the surface. Basis functions for the LUMOs can be derived from $L=1$ spherical harmonics, but we also show the functions derived from the $L=5$ functions, partly to acknowledge the fact that the LUMO of C_{60} has its roots in these higher-order harmonics. In subsequent work, we use the $L=5$ functions as a matter of course. We have explicitly given the basis vectors here (and for the other orientations considered later) for the sake of

TABLE I. Bases used for the LUMO (T_{1u}), HOMO (H_u), and LUMO+1(T_{1g}) orbitals of a pentagon-prone C_{60} molecule. The irreps. are labeled according to their transformation properties. Each set of irreps. is internally self-consistent but unnormalized.

Irrep. (lineage)	Basis function
$T^p_{1ux}(L=1)$	x
$T^p_{1uy}(L=1)$	y
$T^p_{1uz}(L=1)$	z
$T^p_{1ux}(L=5)$	$35z(x^4-6x^2y^2+y^4)-5x(1-14z^2+21z^4)$
$T^p_{1uy}(L=5)$	$5y[28z^4-28xz(x^2-y^2)-(1-7z^2)^2]$
$T^p_{1uz}(L=5)$	$2z(15-70z^2+63z^4)+7x[5(x^2-y^2)^2-4x^4]$
$H^p_{uz^2}(L=5)$	$\sqrt{3}y(5x^4-10x^2y^2+y^4)$
$H^p_{u(x^2-y^2)}(L=5)$	$x(x^2-3y^2)(1-9z^2)+4z(x^2-y^2)(1-3z^2)$
$H^p_{uyz}(L=5)$	$y[1-14z^2+21z^4-12xz(x^2-y^2)]$
$H^p_{uzx}(L=5)$	$3z(x^4-6x^2y^2+y^4)+x(1-14z^2+21z^4)$
$H^p_{uxy}(L=5)$	$y[(y^2-3x^2)(1-9z^2)+8xz(1-3z^2)]$
$T^p_{1gx}(L=6)$	$xz(5-30z^2+33z^4)+20x^2y^2z^2+5(x^2-y^2)^2(x^2-z^2)-4x^6$
$T^p_{1gy}(L=6)$	$y[z(5-30z^2+33z^4)+5x(x^2-y^2)(x^2-y^2+4z^2)-4x^5]$
$T^p_{1gz}(L=6)$	$5yz(5x^4-10x^2y^2+y^4)$

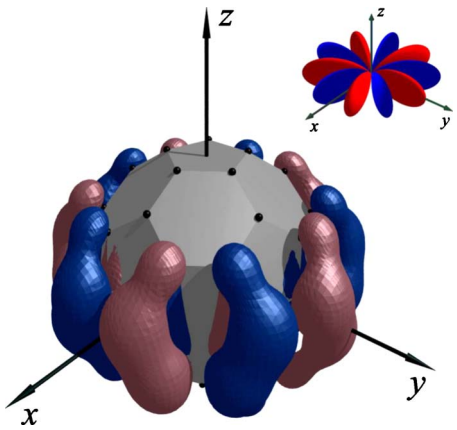

FIG. 3. (Color online) One of the HMOs of H_u symmetry obtained using Ref. 11 and (inset) a comparable plot of the $H^p_{uz^2}$ function given in Table I. The parity of different parts of the orbital is conveyed using color [viz, lighter gray (red in color version) represents a positive lobe of the MO].

completeness and because their definition is not unique. Other, equally valid, basis sets may be found in the literature (see, for example, Refs. 17 and 18) but tend to be arbitrarily labeled. Also, as a basis for the T_{1u} irrep. can be generated using just the $L=1$ harmonics, the $L=5$ counterparts do not tend to be considered. However, these functions have utility here (vide infra).

The basis functions in Table I allow easy assignment of the HMOs. For example, Fig. 3 shows one of the H_u MOs compared to a plot of the $H^p_{uz^2}$ basis function. In this and subsequent plots of MOs, shading (or color in the online version) is used to denote the parity of the orbital. Lighter gray (red in the color version) represents a positive lobe while darker gray (blue in the color version) denotes a negative lobe. The figure clearly shows the correspondence between the two and identifies the MO for subsequent use. The other HMOs of interest can be assigned in the same manner and in this respect the use of the $L=5$ basis functions for the LUMO are essential.

The irreps. shown in Table I will be reducible in C_{6v} symmetry. In order to investigate the characters of the orbitals with respect to the imposed symmetry, we apply symmetry operations of the C_{6v} group to the basis functions representing those orbitals and then look for the component that is unchanged. For example, consider the $H^p_{uz^2}$ function shown in Fig. 3. If we rotate this function by angle ϕ around the z axis, by making the transformation $x \to x\cos\phi + y\sin\phi$, $y \to -x\sin\phi + y\cos\phi$, and $z \to z$, the rotated function can be expanded in the original basis and the coefficient with respect to $H^p_{uz^2}$ found.

The character to be associated with such an operation is thus found to be $\cos\phi\,(16\cos^4\phi - 20\cos^2\phi + 5)$. Therefore, the $H^p_{uz^2}$ function has $\chi(E)=1$, $\chi(C_6)=\frac{1}{2}$, $\chi(C_3)=-\frac{1}{2}$, and $\chi(C_2)=-1$ associated with rotation about the z axis. In a similar fashion, we can find the characters associated with reflection in the mirror planes σ_v and σ_d of the C_{6v} group. We choose the geometry of the surface to be such that the (x,z) plane coincides with a σ_d plane and the (y,z) plane with a σ_v mirror plane. For the $H^p_{uz^2}$ orbital, the characters with respect to the six symmetry planes are found to be: $\chi(\sigma_v)=\{1,-\frac{1}{2},-\frac{1}{2}\}$ and $\chi(\sigma_d)=\{-1,\frac{1}{2},\frac{1}{2}\}$. Overall, the total characters for these two symmetry classes is therefore $\chi(3\sigma_v)=0$ and $\chi(3\sigma_d)=0$. The sums are taken as this is required in order to make use of projection operators to analyze the characters. The full set of orbital characters found in this way is shown in Table II.

TABLE II. Total characters for each C_{6v} symmetry class for the basis functions shown in Table I. The characters for the T_{1u} orbitals have been found using the $L=5$ basis functions.

Irrep.	E	$2C_6$	$2C_3$	C_2	$3\sigma_v$	$3\sigma_d$
T^p_{1ux}	1	$-\frac{2}{5}$	-1	$\frac{2}{5}$	0	0
T^p_{1uy}	1	$-\frac{2}{5}$	-1	$\frac{2}{5}$	0	0
T^p_{1uz}	1	$\frac{43}{25}$	$\frac{29}{25}$	$\frac{11}{25}$	$\frac{54}{25}$	$\frac{54}{25}$
$H^p_{uz^2}$	1	1	-1	-1	0	0
$H^p_{u(x^2-y^2)}$	1	$-\frac{8}{5}$	$\frac{4}{5}$	$-\frac{1}{5}$	$-\frac{9}{5}$	$\frac{9}{5}$
H^p_{uyz}	1	$\frac{2}{5}$	-1	$-\frac{2}{5}$	0	0
H^p_{uzx}	1	$\frac{2}{5}$	-1	$-\frac{2}{5}$	0	0
H^p_{uxy}	1	$-\frac{8}{5}$	$\frac{4}{5}$	$-\frac{1}{5}$	$\frac{9}{5}$	$-\frac{9}{5}$
T^p_{1gx}	1	$\frac{17}{25}$	$-\frac{16}{25}$	$-\frac{8}{25}$	$\frac{9}{25}$	$\frac{9}{25}$
T^p_{1gy}	1	$\frac{17}{25}$	$-\frac{16}{25}$	$-\frac{8}{25}$	$-\frac{9}{25}$	$-\frac{9}{25}$
T^p_{1gz}	1	1	-1	-1	0	0
Combinations						
$\frac{1}{\sqrt{2}}(H^p_{u(x^2-y^2)}+H^p_{uxy})$	1	$-\frac{8}{5}$	$\frac{4}{5}$	$-\frac{1}{5}$	0	0
$\frac{1}{\sqrt{2}}(H^p_{u(x^2-y^2)}-H^p_{uxy})$	1	$-\frac{8}{5}$	$\frac{4}{5}$	$-\frac{1}{5}$	0	0
$\frac{1}{\sqrt{2}}(T^p_{1gx}+T^p_{1gy})$	1	$\frac{17}{25}$	$-\frac{16}{25}$	$-\frac{8}{25}$	0	0
$\frac{1}{\sqrt{2}}(T^p_{1gx}-T^p_{1gy})$	1	$\frac{17}{25}$	$-\frac{16}{25}$	$-\frac{8}{25}$	0	0

The resulting characters can be used to decompose the icosahedral irreps. in terms of the C_{6v} irreps. Thus, the $H^p_{uz^2}$ and T^p_{1gz} functions decompose to $\frac{1}{2}E_1$. More importantly, if we assume that the interaction with the surface is symmetry dependent then, using an argument similar to that used in crystal field theory, we can expect that the functions with the same transformation properties will be degenerate as a result of the surface interaction. Thus, we expect the (T^p_{1ux}, T^p_{1uy}) LUMO pair and (H^p_{uyz}, H^p_{uzx}) HOMO pair to be degenerate.

Further degeneracy is not immediately apparent. However, singling out orbitals with unique character, such as $H^p_{uz^2}$ and T^p_{1gz}, suggests which orbitals should be checked in combination. This yields two further sets of orbital pairs with the same transformation properties and therefore the same energy, as shown in Table II. The overall result is that the interaction of the C_{6v} surface with a pentagon-prone C_{60} molecule causes a reduction in degeneracy such that

$$T_{1u} \to \{(T^p_{1ux}, T^p_{1uy}), T^p_{1uz}\},$$

$$H_u \to \{H^p_{uz^2}, (H^p_{uyz}, H^p_{uzx}), (H^p_{u(x^2-y^2)} + H^p_{uxy}, H^p_{u(x^2-y^2)} - H^p_{uxy})\},$$

TABLE III. Bases used for a hexagon-prone molecule. The irreps. are again labeled using functions that share their transformation properties, except for H_u (which are simpler in the form shown) and unnormalized but self-consistent.

Irrep. (lineage)	Basis function
$T^h_{1ux}(L=1)$	x
$T^h_{1uy}(L=1)$	y
$T^h_{1uz}(L=1)$	z
$T^h_{1ux}(L=5)$	$35z[2(x^2-y^2)(4-3x^2)-7x^4+11y^4]+\sqrt{5}x[14(4y^2-z^2)(1-4x^2)+7(1-5z^2)(3-5z^2)-2]$
$T^h_{1uy}(L=5)$	$140xyz(1+2y^2-5z^2)-\sqrt{5}y[100-56y^2(5x^2+y^2)-35(1+z^2)^2]$
$T^h_{1uz}(L=5)$	$35x(9z^2-1)(x^2-3y^2)-2\sqrt{5}z(15-70z^2+63z^4)$
$H^h_{u1}(L=5)$	$10z[x^2(11x^2-4)-y^2(y^2+30x^2-4)]+\sqrt{5}x[96-28x^2(x^2+5y^2)-7(3+z^2)^2]$
$H^h_{u2}(L=5)$	$3\{5x(1-14z^2+21z^4)-\sqrt{5}z[(1-z^2)(1-9z^2)+8x^2(2-3x^2)]\}$
$H^h_{u3}(L=5)$	$-3\sqrt{14}y\{10xz(x^2-y^2)-\sqrt{5}[1-8z^2+11z^4+2x^2(x^2-3y^2)]\}$
$H^h_{u4}(L=5)$	$2\sqrt{14}y\{\sqrt{5}xz(8-x^2-23y^2)-5[x^2(x^2-3y^2)+z^2(3-5z^2)]\}$
$H^h_{u5}(L=5)$	$3\sqrt{35}y(3x^2-y^2)(9z^2-1)$
$T^h_{1gx}(L=6)$	$y\{z[8y^2(5x^2+y^2)-5(1+z^2)^2+28z^4]+\sqrt{5}x[(1-4y^2+z^2)(1-11z^2)+4z^2]\}$
$T^h_{1gy}(L=6)$	$xz[(2x^2-3z^2)(3-7x^2-5y^2)+(1-2y^2)(1+14y^2)]+\sqrt{5}[(x^2-y^2z^2-2x^4)(3-11z^2)+2x^2(x^2-11y^2z^2)]$
$T^h_{1gz}(L=6)$	$y(3x^2-y^2)[4x(x^2-3y^2)-\sqrt{5}z(3-11z^2)]$

$$T_{1g} \to \{(T^p_{1gx}+T^p_{1gy}, T^p_{1gx}-T^p_{1gy}), T^p_{1gz}\}, \tag{2}$$

where parentheses indicate degenerate (unnormalized) pairs.

D. Hexagon- and double-bond-prone C_{60}

We have performed analogous calculations for the case when a hexagonal face is pointing toward the surface and when a carbon-carbon double bond is prone to the surface. For both cases, we generate new basis functions for the irreps. using the same method as before, viz, diagonalization of the suitably rotated icosahedral potential given by Eq. (1). The functions thus obtained and used here are given in Tables III and IV, where suitable superscripts have been used to distinguish the different orientations.

Once again, analysis of these functions via their characters reveals the degeneracies to be expected as a result of surface interaction. It is found that the (unnormalized) combinations required for adsorption at a site of C_{6v} symmetry are

$$T_{1u} \to \{(T^h_{1ux}, T^h_{1uy}), T^h_{1uz}\},$$

$$H_u \to \{(aH^h_{u1}+a'H^h_{u2}, -b'H^h_{u3}+bH^h_{u4}), (-a'H^h_{u1}+aH^h_{u2}, bH^h_{u3}+b'H^h_{u4}), H^h_{u5}\},$$

$$T_{1g} \to \{(T^h_{1gx}, T^h_{1gy}), T^h_{1gz}\} \tag{3}$$

for the hexagon-prone case, where $a=\sqrt{\sqrt{9289}+53}$, $b=\sqrt{a^2+9}$, $a'=\sqrt{a^2-106}$, and $b'=\sqrt{a^2-115}$, and parentheses again indicate degeneracy.

Similarly, for the double bond-prone case, we find

$$T_{1u} \to \{(T^{db}_{1ux}+T^{db}_{1uy}, T^{db}_{1ux}-T^{db}_{1uy}), T^{db}_{1uz}\},$$

$$H_u \to \{(H^{db}_{uz^2}, H^{db}_{u(x^2-y^2)}), (H^{db}_{uyz}+H^{db}_{uzx}, H^{db}_{uyz}-H^{db}_{uzx}), H^{db}_{uxy}\},$$

$$T_{1g} \to \{(T^{db}_{1gx}+T^{db}_{1gy}, T^{db}_{1gx}-T^{db}_{1gy}), T^{db}_{1gz}\}. \tag{4}$$

TABLE IV. Bases for a double bond-prone molecule. The other functions not shown are generated using consecutive cyclic permutations $x \to y \to z \to x$. Each set is once again self-consistent but unnormalized.

Irrep. (lineage)	Basis function
$T^{db}_{1ux}(L=1)$	x
$T^{db}_{1ux}(L=5)$	$x[7x^4+70y^2z^2-5+7\sqrt{5}(1-3x^2)(y^2-z^2)]$
$H^{db}_{uz^2}(L=5)$	$8\sqrt{3}xyz[1-3z^2-\sqrt{5}(x^2-y^2)]$
$H^{db}_{u(x^2-y^2)}(L=5)$	$-8xyz[3(x^2-y^2)+\sqrt{5}(1-3z^2)]$
$H^{db}_{uyz}(L=5)$	$x[(1-3x^2)(9-11x^2)-3(y^2-z^2)^2-2\sqrt{5}(1-3x^2)(y^2-z^2)]$
$T^{db}_{1gx}(L=6)$	$yz\{2(1-11x^2)(y^2-z^2)-\sqrt{5}[(1-3x^2)^2-3(y^2-z^2)^2]\}$

The final step is to make the connection between the basis functions and their HMOs given in the pentagon-prone orientation. This is done by simply rotating the functions into the pentagon-prone frame and expanding in the pentagon-prone basis functions.

III. ORBITAL PICTURES AND STM SIMULATIONS

The expressions for the HMOs obtained in the last section can be used to create pictures of the orbital combinations that are expected to be produced when a C_{60} molecule interacts with a surface at a site of C_{6v} symmetry. Accompanying simulations of STM images can then be obtained using the simple tunneling theory approach developed by Tersoff and Hamann.[19] Their work suggests that the tunneling current I measured during STM is approximately proportional to the density of the electronic surface states evaluated at the position of the STM tip $\mathbf{r}_0$. That is to say

$$I \propto \sum_{\nu} |\psi_{\nu}(\mathbf{r}_0)|^2 \delta(E_{\nu} - E_F), \tag{5}$$

where ψ_{ν} is the wave function of a surface state of energy E_{ν}, E_F is the Fermi energy, and ν runs over all the available surface states. In imaging the LUMO, therefore, we assume that sufficient positive bias is applied to the surface so that the current will be proportional to the electron density $\rho_{\mathrm{LUMO}}(\mathbf{r}_0)$ evaluated at $\mathbf{r}_0$, given by

$$\rho_{\mathrm{LUMO}}(\mathbf{r}_0) = \sum_{\nu=x,y,z} |T_{1u\nu}(\mathbf{r}_0)|^2, \tag{6}$$

where the sum extends over all the degenerate orbitals. It is a simple matter to evaluate Eq. (6) in a plane parallel to the (x,y) plane and hence generate a "constant-height" STM image. It is also relatively easy to extend the calculations to create plots which show the tip height required to maintain a constant tunneling current, thus producing constant current simulations.

Equation (6) is readily generalized to the HOMO and LUMO+1. These three sets of orbitals are expected to be well separated in energy and therefore imaged at three different applied biases in an STM experiment. However, it should be noted that if the C_{60} is strongly perturbed by the surface then the degeneracy will be reduced and the split components could overlap in the STM image. Here, we will assume that such complications are not present and that, provided the correct bias is chosen, the nondegenerate and degenerate pairs indicated in Eqs. (2)–(4) can be separately imaged. In this case, Eq. (6) is again appropriate provided we sum over only those orbitals deemed to be degenerate (and that the surface site has C_{6v} symmetry). Of course, group theory gives no indication of the magnitude or order of splitting and therefore which orbital combinations appear at higher biases compared to the others. Our aim is to simply indicate what could be observed provided there is no further overlapping of the orbitals. This does not mean that every image inferred should be observable; even in the absence of interference from adjacent orbital sets, some of the split components will produce very weak STM images because they present only small electron densities in the general direction of the STM tip.

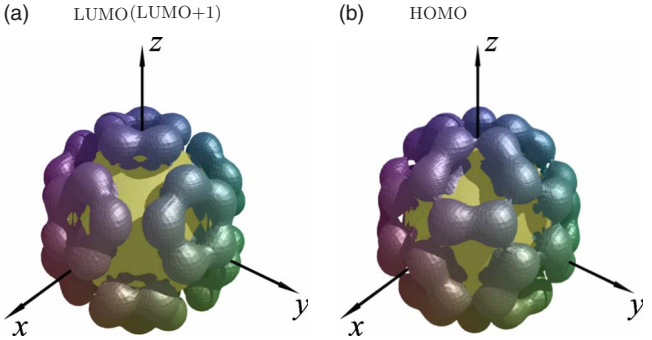

FIG. 4. (Color online) Orbital representations of the sums of the squares of the frontier orbitals for the case of complete degeneracy.

The actual image observed using STM depends on many experimental parameters and it is not possible to generate a single definitive image to predict the outcome of an STM experiment. These parameters are usually adjusted to produce images that match those observed as closely as possible. By starting from Eq. (6), it clear that the best STM image that could be produced would be one that accurately reflects the quantity $\rho_{\mathrm{LUMO}}(\mathbf{r}_0)$ as experienced by the STM tip. In other words, our ideal STM image would be one that gives a good representation of the total electron density as it would be observed along the z direction. One can then extrapolate the images obtained to less than ideal conditions that will produce a more realistic representation of observed images. We illustrate this using the simple, noninteracting case when each set of orbitals is degenerate.

The total electron densities in the presence of degeneracy are shown in Fig. 4. For the LUMO and LUMO+1, the representations are identical and feature a concentration of the electron density within the pentagonal face of the molecule. On the other hand, the HOMO sees its electron density associated with the carbon-carbon double bonds. It is noteworthy that these electron distributions are often used as a basis for the interpretation of experimental STM images; satisfactory agreement leading to the conclusion that the orbitals have retained their degeneracy and so there must be only a weak or negligible surface-C_{60} interaction. We shall examine the validity of this conclusion later. Another important point is that because the LUMO and LUMO+1 orbitals both have T_1 symmetry, differing only in their parity, they would

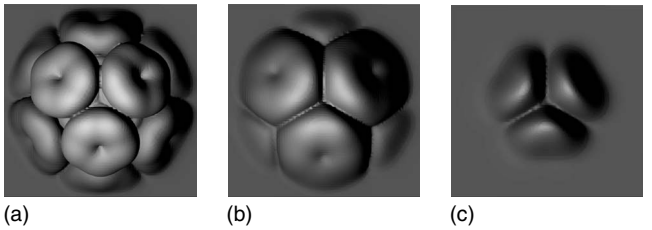

FIG. 5. STM simulations of the (rotated) electron density shown in Fig. 4(a). In (a), a large tunneling current is assumed. Subsequent images (b) and (c) correspond to consecutive 22-fold reductions in the current.

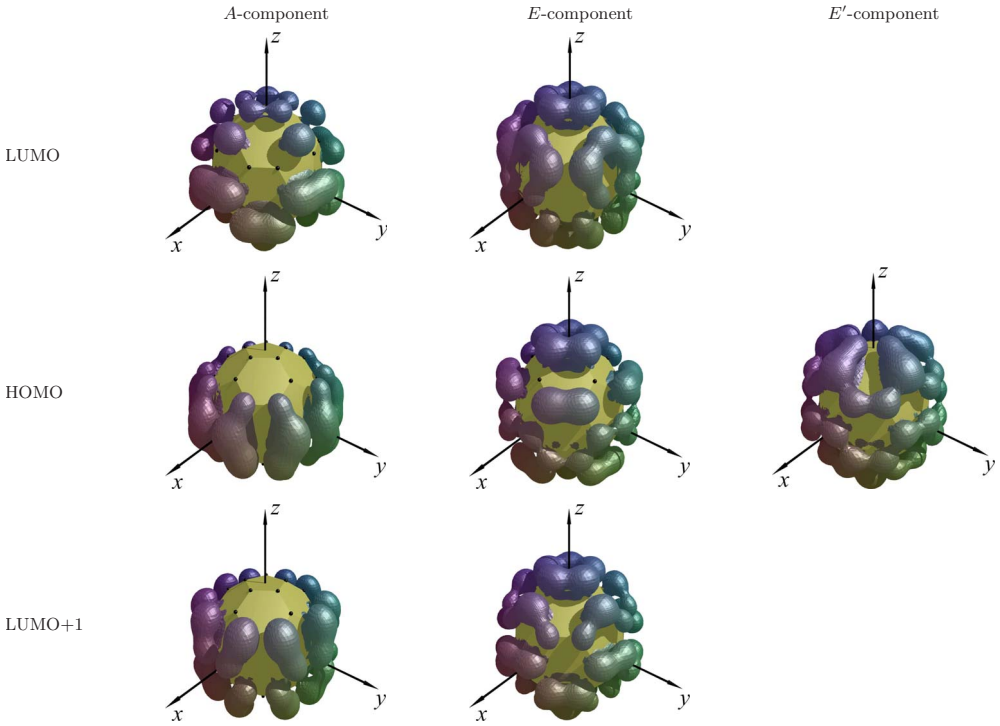

FIG. 6. (Color online) Pictorial representation of the total electron densities $\Sigma_\nu|\psi_\nu|^2$ for the different components arising after a C_{6v} surface interaction. The molecule has a pentagonal face pointing toward the surface, located in the $-z$ direction. For the HOMO, the combination (H^p_{uyz}, H^p_{uzx}) corresponds to the first degenerate pair E.

produce identical STM images. As these two sets of orbitals are close in energy, there is the possibility that features arising due to these orbitals could be incorrectly assigned.

Now consider an idealized STM image arising from the distribution shown in Fig. 4(a). We use Eq. (6) to make an implicit plot in which we fix the tunneling current and vary the height of the STM tip in the direction perpendicular to the substrate in order to maintain the current for different values of the coordinates in the plane of the substrate, i.e., we make a constant-current simulation. As we want to accurately reflect the electron density shown, we make the tunneling current large. We also ignore any effects due to the finite size of the STM tip so that we effectively "etch out" a profile that closely resembles the electron distribution shown. The "images" produced show details that could only be produced by an infinitely thin tip that is allowed to penetrate the fullerene cage—a process that will not occur in a real experiment. A high-current STM image produced under these ideal conditions is shown in Fig. 5(a), where we have oriented the molecule so that a hexagonal face is presented to the STM tip.

The image in Fig. 5(a) clearly gives a good representation of what the LUMO electron distribution looks like (lighter areas correspond to larger tip-surface distances). Note that this image has been generated using added lighting effects to enhance the three-dimensional quality of the picture. This is an approach commonly used to enhance real STM data and one which we will adopt from now on. The figure implies that the brighter, central parts of the image arising from the three "upper" lobes of the LUMO are closest to the observer. Thus, we can expect these parts to be more prominent in real STM images obtained from a C_{60} molecule oriented in this manner. In Fig. 5(b), we show the image obtained when the tunneling current is reduced by a factor of 22. Reduced current means the tip-surface distance is increased and the device is responding to the smaller electron densities in the "outer" regions of the LUMO. In this image, the central three lobes feature more strongly.

The result of a further 22-fold reduction in tunneling current (~500-fold overall) is shown in Fig. 5(c). Now the three upper lobes dominate the image, producing an image reminiscent of a three-leafed clover. This latter image is remarkably similar to real STM images appearing in the literature.[2,20–26] For example, Fig. 5(c) is almost identical to images obtained by Silien *et al.* [Fig. 1(a), Ref. 2] from C_{60} molecules adsorbed onto a Cu(111) surface using a bias of +2.0 V, which corresponds to just the right potential to image the LUMO/LUMO+1 orbitals.

Our simulation in Fig. 5(b) can also be compared to high-resolution STM images and corresponding density-functional-theory (DFT) simulations of C_{60} on a Pt(110) surface in Fig. 10(A) of Casarin *et al.*[15] The geometry of Casarin *et al.*'s results is not quite the same as ours with a hexagon rotated slightly from the center of the image (an orientation which these authors call M1, as shown in their Fig. 3). Also, their C_{60} molecule sits over a "bridge site," which does not correspond to the C_{6v} symmetry we assume. However, the symmetry of the surface is irrelevant as we are assuming total degeneracy. Allowing for the slight difference in molecular orientation, our results in Fig. 5(b) bear a strong

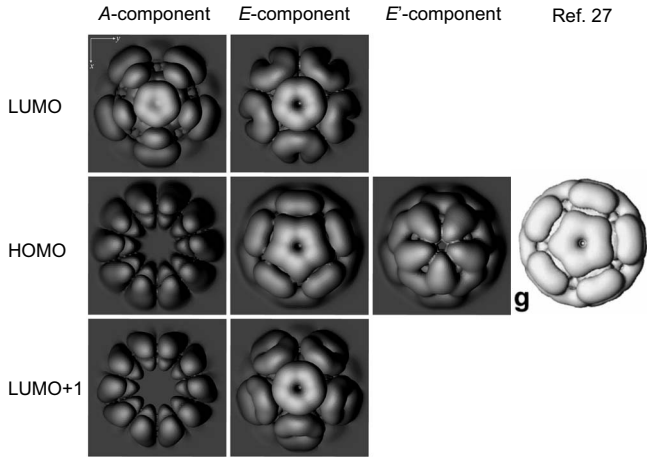

FIG. 7. Idealized STM simulations of the orbital combinations given in Eq. (2) and shown in Fig. 6. The C_{60} molecule is oriented into a pentagon-prone configuration and the perturbing surface site is assumed to have C_{6v} symmetry. For the HOMO, the combination (H^p_{uyz}, H^p_{uzx}) corresponds to the first degenerate pair E. Also shown is a DFT simulation taken from Fig. 2 of Pascual *et al.* (Ref. 27).

resemblance to both the STM images and DFT simulations. This gives us confidence that the simple molecular-orbital methods used here give similar results to the more sophisticated DFT calculations.

The series of images in Fig. 5 indicate that idealized, high-current simulations are useful to consider. While they do not depend on any of the experimental parameters upon which captured STM images depend so cannot be expected to reproduce observed images directly, they can show subtle differences in electron distribution and can be used as a guide to identification of which combinations of orbitals could be responsible for features appearing in actual STM images. For these reasons, we use these idealized simulations from this point onward.

A. Pentagon-prone images

We first consider a C_{60} molecule oriented in the pentagon-prone configuration. Figure 6 collects together a set of images representing the total electron densities associated with the combinations listed in Eq. (2). Idealized STM simulations of these combinations are presented in Fig. 7.

One of the interesting features of the images shown in Figs. 6 and 7 is that the E components arising from each of the three sets of orbitals all have a pentagonal lobe oriented along the z axis. All of these would be expected to produce a similar image when viewed via STM, each appearing as a fivefold symmetric ring, possibly with a dip in the middle. Such images have been observed and documented in the literature.[5,8,27] Of particular interest here are the experimental results of Pascual *et al.*,[27] observed at a bias of 2 V in STM experiments on isolated C_{60} molecules on Si(111). The authors claim that their results arise from the E component of the HOMOs. However, we would not expect a HOMO-related feature to be imaged at such a bias. Indeed, the result in part c of their Fig. 2 shows strong similarities with our result for the E components of the LUMO orbitals shown in Fig. 7. This could indicate that an incorrect assignment may have occurred. Interestingly, the authors of Ref. 27 themselves create a simulated image of the doubly degenerate orbitals they deem responsible for their observation, using an *ab initio* method based on DFT in the local-density approximation. Part g of their Fig. 2,[27] which we have reproduced in Fig. 7 can be seen to exactly match our simulation of the HOMO E orbital. This again gives us reassurance that the methods used here, though simple, are consistent with more complex methods of calculation. In fact, the agreement with the simulation and experimental observation of Pascual *et al.* suggests that the group theoretical technique used here gives a sound rationale for the surface-induced splitting predicted by Eq. (2) (in Ref. 27, the surface interaction is modeled by applying a strain along a particular rotational axis).

It should be noted that the three A components are expected to be only weakly visible via STM. This is because they only have small electron densities in the z direction, as apparent from Fig. 6. Therefore, it is possible that the splitting induced by an adsorbing surface may go unnoticed in the dI/dV data gathered in a scanning tunneling spectroscopy (STS) experiment. In addition, the HOMOs could appear to be split into two peaks rather than three. To our knowledge, the predicted HOMO E' component (which would have the appearance of a five-petaled flower) has not been observed experimentally. Of course, its observation would give good support to the validity of the theory presented here but it is also possible that this particular orbital combination may be present but difficult to observe. First, it requires that the C_{60} adsorbs onto the surface with a pentagonal face pointing downwards. It has been speculated that this might be an energetically favorable adsorption geometry based on an analogy with ferrocene. In practice, however, the observation of fivefold-symmetric features seems to be rather rare. Second, there is also the possibility that the surface interaction could shift the E' component to a bias region obscured by the nearby HOMO-1 orbitals. According to HMO theory,[28] these latter orbitals are of $G_g \oplus H_g$ symmetry, and the HOMO-HOMO-1 gap is only $\sim 57\%$ larger than the equivalent LUMO-LUMO+1 gap in the free molecule. If bond alternation is included, this figure drops to just 13% (Ref. 12) so overlap between the HOMO and HOMO-1 orbitals could well be expected to arise in a surface-perturbed C_{60} molecule.

B. Hexagon-prone images

We repeat the calculations above for a hexagon-prone molecule with the surface-induced splitting detailed in Eq. (3). Figure 8 collates the total electron densities and the corresponding idealized STM simulations are presented in Fig. 9. It is immediately obvious that these results could not have been obtained from those for the pentagon-prone case by rotating the viewing angle. As for the pentagon-prone case, the E components from each of the three sets of orbitals all produce similar STM images, an image very similar to those shown in Fig. 5 for an unperturbed set of C_{60} LUMOs (the "three-leafed clover"). Therefore, there is, once again, the possibility that an incorrect assignment could occur when examining experimental data.

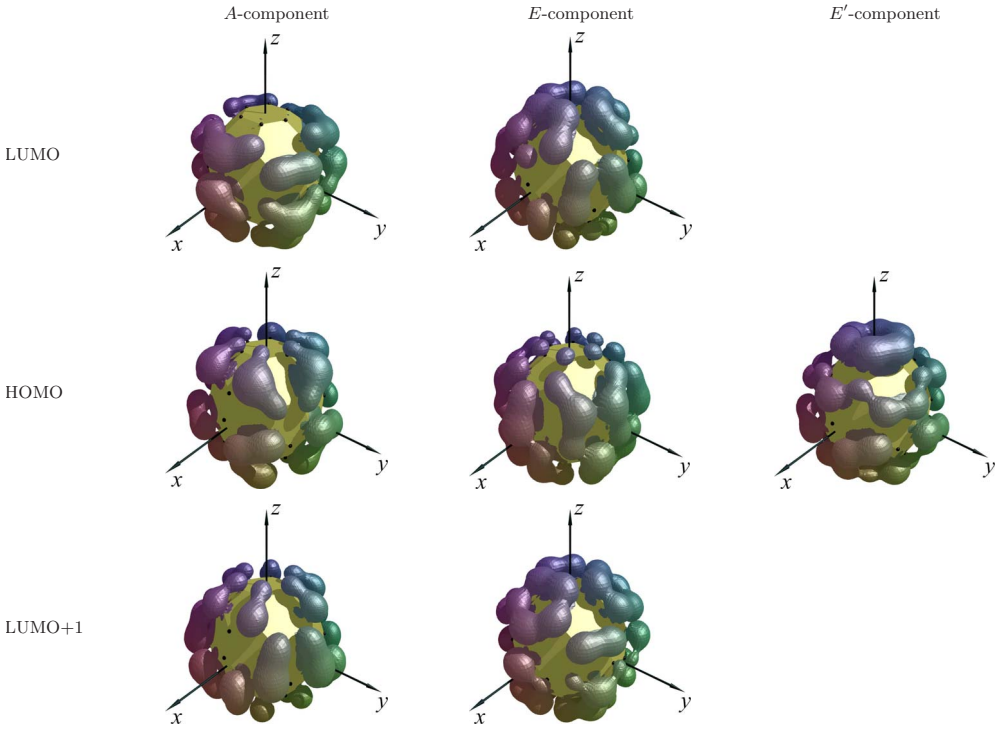

FIG. 8. (Color online) Pictorial representations of the total electron densities for a hexagon-prone molecule (as for Fig. 6). For the HOMO, the E component corresponds to the $(aH^h_{u1}+a'H^h_{u2},-b'H^h_{u3}+bH^h_{u4})$ orbital pair indicated in Eq. (3).

It is also seen that the A components in Fig. 8 will again tend to produce weaker signatures in the resultant STM images compared to the other components. Two of them (from the HOMO and LUMO+1) are expected to appear as six-petaled flowers in STM images but the third (the LUMO A component) has apparent threefold symmetry and would have a more triangular appearance, as shown in Fig. 10. Triangular features, thought to arise from the LUMO of C_{60}, have been observed[9] in potassium-doped C_{60} monolayers on Au(111). The added complication here of the alkali metal prevents unequivocal assignment of such features solely to the A component of a set of hexagon-prone LUMOs. However, we do note that of all the images generated in the current (undoped) work, this particular arrangement is the only one to produce an even vaguely trigonal image.

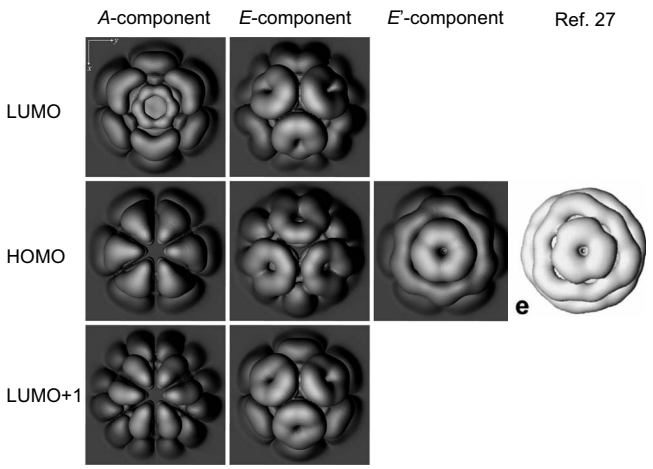

FIG. 9. Idealized STM simulations of the orbital combinations given in Eq. (3) and shown in Fig. 8. The C_{60} molecule is oriented into a hexagon-prone configuration and the perturbing surface site is assumed to have C_{6v} symmetry. For the HOMO, the combination $(aH^h_{u1}+a'H^h_{u2},-b'H^h_{u3}+bH^h_{u4})$ corresponds to the first degenerate pair E. Also shown is a DFT simulation taken from Fig. 2 of Pascual *et al.* (Ref. 27).

Figure 9 also shows the simulated image of a doubly degenerate orbital generated by Pascual *et al.* using DFT (Ref. 27) (part e of their Fig. 2). Their image can be seen to be almost identical to our simulation of the HOMO E' component. Both simulations agree well with the experimentally observed STM images (part a of their Fig. 2). This again gives us confidence in the methods used in the current work. Furthermore, it is a combination which the authors of Ref. 27 appear to observe with some clarity in high-resolution STM images of individual C_{60} molecules on Si(111). Surprisingly, they state that their image was recorded using a bias of 2 V. We note that this is not a bias at which one would expect to find a HOMO of C_{60}. At lower resolution, the E' component

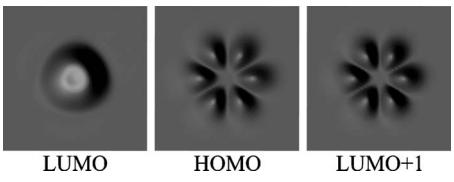

FIG. 10. Comparison of some low-current STM simulations of the hexagon-prone A components shown in Fig. 9. The current used corresponds to that used in Fig. 5(c).

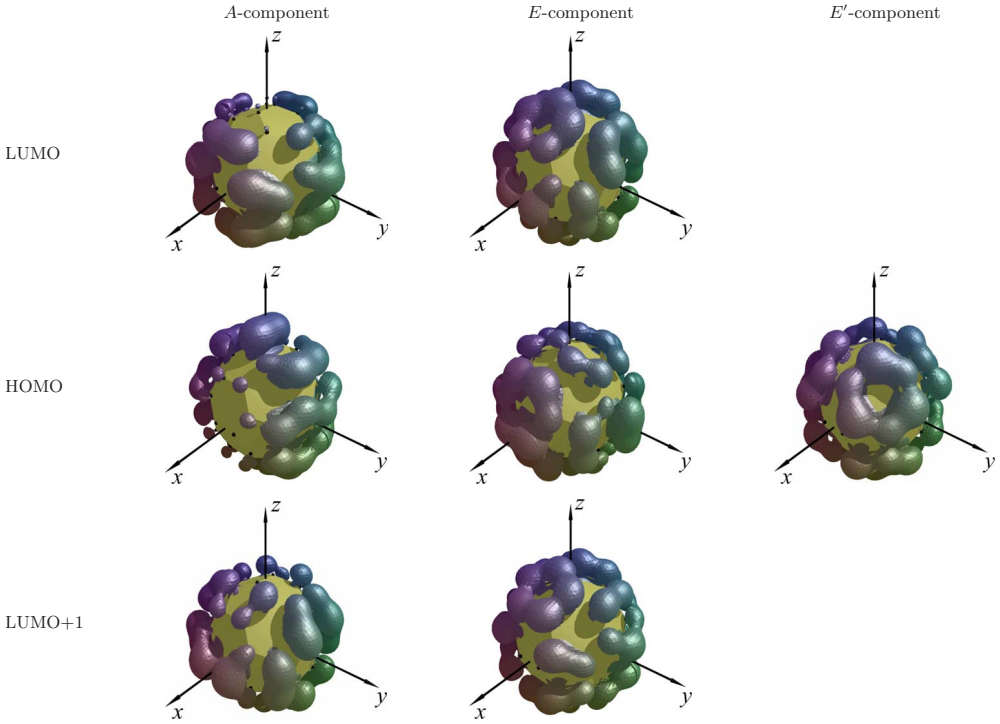

FIG. 11. (Color online) Pictorial representations of the total electron densities for a double bond-prone molecule perturbed by a C_{6v} surface. The HOMO E component corresponds to the pair $(H^{db}_{uyz}+H^{db}_{uzx}, H^{db}_{uyz}-H^{db}_{uzx})$ given in Eq. (4).

would give the appearance of a hollow hexagonal crater, perhaps matching those observed by Altman *et al.*[8] using a monolayer of C_{60} molecules on Au(111). In this latter work, however, the HOMO image was recorded at a more convincing bias of −2 V. This suggests that the bias in Ref. 27 could be wrongly reported.

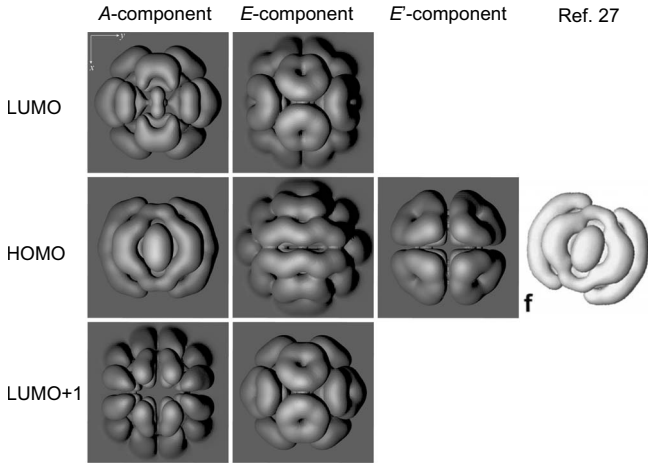

FIG. 12. Idealized STM simulations of the orbital combinations given in Eq. (4) and shown in Fig. 11. The C_{60} molecule is oriented into a double bond-prone configuration and the perturbing surface site has C_{6v} symmetry. For the HOMO, the E component corresponds to the $(H^{db}_{uyz}+H^{db}_{uzx}, H^{db}_{uyz}-H^{db}_{uzx})$ orbital pair. Also shown is a DFT simulation taken from Fig. 2 of Pascual *et al.* (Ref. 27).

C. Double-bond-prone images

The final case considered here is that of a C_{60} molecule oriented so that a double bond is pointing toward the surface, where we use the surface-induced splitting given in Eq. (4). Figure 11 collates the total electron densities and the corresponding idealized STM simulations are presented in Fig. 12.

At first sight, it would appear from Fig. 12 that, in contrast to the pentagon-prone and hexagon-prone cases, the E components from the three sets of orbitals in the double bond-prone case will not all produce similar STM images. This would indeed be the case at high resolution. However, a more realistic simulation using a lower tunneling current highlights only the central parts of the images shown in Fig. 12 and this produces a virtually identical image in each case; a double-lobed image akin to that produced by the unperturbed distribution itself [as given in Fig. 4(a)]. In fact, lower current simulations of each of these orbital pairs produce double-lobed images that closely match those observed in a series of papers by Crommie *et al.*[9,21,29,30] It is noteworthy that in this series, the double-lobed images were recorded at a bias of 2 V on an undoped Ag(001) surface and at ~−0.1 V on a Au(111) surface with potassium doping. In contrast, Schull *et al.*[26] have recorded similar double-lobed images (as well as other orientations due to the formation of an orientationally ordered 7×7 superstructure in the C_{60} monolayer) using a bias of 1.5 V on an undoped Au(111) surface. Assuming these features all arise from the E component of the LUMO, this suggests that this orbital pair re-

quires a bias of 1.5–2 V for imaging on undoped metallic surfaces. Of course, the shift to values near 0 V upon doping is entirely consistent with the doping electrons taking up residence within the LUMO.

Similar double-lobed images have also been observed[31] at a sample bias of −2 V and can therefore be assigned to a HOMO origin. In fact, several interesting images recorded at this bias value are presented in Ref. 31 and are, therefore, potentially HOMO related. In one particular image (Fig. 5), the double-lobed images (arbitrarily labeled as due to molecules of type "B" in Ref. 31) were simultaneously observed alongside other molecules having a striped appearance (type "A"). It is interesting to observe that the HOMO *A* component shown in Fig. 12 would produce a similarly striped image when observed at low resolution. If these *A* and *E* components are responsible for the images observed then there is the question of how they could simultaneously appear in a single STM image at one particular bias.

The obvious suggestion to make is that individual molecules are experiencing additional site-specific perturbations which could bring either the *A* or *E* component into resonance with the STM tip even though the bias has not changed. Certainly, the complex nature of the Si(111)-$\sqrt{3}\times\sqrt{3}$-Ag surface used in Ref. 31 would lend some credence to this explanation. However, one would still expect the distribution of A- and B-type molecules to follow a regular pattern on this surface and not be randomly distributed as observed. The basis of such an expectation, on the other hand, is that adsorption at equivalent sites should affect the adsorbed C_{60} units in an identical manner. This would be approximately true if the interaction with the surface is strong and the effects of neighboring C_{60} molecules can be ignored. However, the authors of Ref. 31 believe the interaction between the Si(111)-$\sqrt{3}\times\sqrt{3}$-Ag surface and adsorbed molecules to be weak because of the long diffusion length inferred for C_{60} molecules on the surface. If this is the case, the surface-induced splitting is expected to be weak and the HOMO-derived components should all be close in energy and therefore imaged at nearly the same bias. At the same time, if the surface interaction is weak, the importance of the effects of neighboring C_{60} molecules is enhanced. If each surface site has threefold symmetry, then the same surface interaction will be present when any individual C_{60} molecule is rotated by 120°. The strongest C_{60}—C_{60} interactions, however, will be governed by the orientations of six nearest-neighbors, each of which could be in one of three "equivalent" differently aligned configurations. The complexity of this latter interaction could lead to random distributions of type A and B molecules over the surface.

The HOMO *A* component shown in Fig. 12 is yet another example of an almost perfect match to one of the images generated by Pascual *et al.*[27] using *ab initio* methods, which we reproduce in Fig. 12 (part f of their Fig. 2),[27] and also a good match to their experimental STM image (part c of their Fig. 2). Again this gives us good reason to trust the method of calculation used here. More importantly, the authors of Ref. 27 recorded high-resolution STM images of C_{60} molecules that correlate very well with the HOMO *A*-component simulation in Fig. 12. Furthermore, the appearance of the observed high-resolution STM image confirms that lower resolution experiments would indeed detect C_{60} molecules with striped features. It is also interesting to note that the −1.5 V bias used to record the high-resolution STM images [on a Si(111)-(7×7) surface] is fairly consistent with the −2 V bias used[31] in the lower-resolution study.

The HOMO E' component for the double bond-prone orientation appears to have fourfold symmetry and, at lower resolution, this orbital pair would produce an STM image resembling a four-petaled flower. To the best of our knowledge, such an image has not been recorded in any STM experiment on C_{60} and attributed to the HOMO orbitals. That is not to say that fourfold symmetry has not been observed in STM images of C_{60}. A good example of such a feature can be found in the images of (nominally) K_3C_{60} formed by potassium doping C_{60} on Au(111).[9] These fourfold symmetric features look very similar to those produced by the E' component but were recorded at a bias of +0.1 V, not a bias at which HOMO orbitals are to be expected. It should be noted that the LUMO+1 *A* component, although weak, also produces a similar image at low resolution. In fact, the image is slightly rectangular in distribution rather than square and constitutes an even better match to the observed STM than the HOMO component does. Furthermore, as doping has the effect of shifting the orbitals to more negative biases, it might be plausible that a split LUMO+1 orbital could appear near 0 V in these images.

The only component not mentioned so far is the *A* component derived from the set of LUMO orbitals. This is another component that would be only weakly visible in STM images and so may be overlooked or disguised by other orbitals. At low resolution, the central lobe shown in Fig. 12 becomes more prominent resulting in a simple oval-shaped image. As such featureless images are often observed in STM studies, there seems to be little point attempting to find experimental evidence for the occurrence of this component. This situation, of course, would change if the orbital were to be observed via high-resolution STM since, at higher resolution, the appearance of the orbital would be very characteristic indeed. Thus, it is hoped that the images presented in the current work, idealized as they are, may be useful in identifying features that have yet to be observed in STM experiments on C_{60}. This is especially so as the experimental techniques and equipment used become more sophisticated and thus capable of resolving intramolecular features in more detail and with greater certainty.

IV. SUMMARY AND CONCLUSIONS

STM is a very powerful technique for atomic-resolution studies of molecules adsorbed on surfaces. C_{60} is a particularly attractive candidate for surface-adsorbed imaging because of its large size and due to the general interest in this molecule. The image recorded via STM should give a good indication of the orientation of the adsorbed molecule, provided molecular rotation is suppressed. One would also expect that the STM image should depend on the nature of the interaction between the C_{60} molecule and the surface. In the extreme limit where there is no surface interaction, the STM images would be independent of the surface used and would

match those expected from unperturbed, icosahedral molecules. Thus, observations matching the unperturbed distributions (Fig. 4) are often used to indicate that the interaction with the surface is weak. In the current work, we have seen that this inference may not necessarily be valid and that this could lead to incorrect assignments.

In this paper, we have not made any assumptions about the strength of the surface interaction present for any given surface. What we have assumed is that the adsorption site has a particular symmetry which will have an effect on the relevant orbitals causing them to lose their degeneracy. Using group theoretical methods we have determined the nature of this degeneracy loss and used the results to visualize the split components as they might appear through STM. While we cannot determine the bias at which the results would be obtained for a given surface, we do expect all the images we derive to be observed at some bias. As the images we have generated are, on the whole, very different from each other, we have therefore used the analysis of real STM data to reveal information on the nature of the C_{60}-surface interaction (rather than fixing a surface interaction to predict STM data).

Implicitly, our analysis requires that the surface interaction should be sufficiently strong that the STM can respond to the split components separately, without interference from the other components. This, however, does not make the results valid only in the strong-interaction regime—for weaker interactions the images can be superimposed to see what would be observed if the splitting is small.

In several instances we have seen that even if the splitting is strong, one component may have the same appearance via low-resolution STM imaging as the unperturbed, degenerate case. This, of course, arises because the noncontributing component(s) have weak electron densities in the tip direction. Therefore, even if the surface interaction is strong and causes a large splitting in the normally degenerate orbitals, an STM image may not show this, leading to the erroneous conclusions that the orbitals have retained their degeneracy and thus that the interaction is weak. To try to anticipate such occurrences we have attempted to generate a "complete set" of images that could be obtained if a suitably oriented C_{60} molecule is adsorbed at a surface site possessing C_{6v} symmetry. In some ways, the approach has been very crude but it does maintain a level of completeness which makes the images internally self-consistent. Justification for the techniques used lies in the good agreement observed with actual STM images appearing in the published literature and the similarly good agreement with published *ab initio* calculations, such as those in Ref. 27. This implies that *ab initio* methods are not always necessary to provide simulations of observed STM images. Our techniques could, of course, be readily extended to surface sites having other symmetries and to C_{60} molecules having other orientations.

Not all of the simulated STM images that we have presented here seem to have been observed experimentally but there are many reasons that could account for this, as we have discussed already. One of the important reasons is that the image may be too weak to be observed. This becomes even more apparent if constant-height simulations are made and used to estimate the relative tunneling currents that would arise from the split components. Such comparisons suggest that the weaker components may not appear in STS experiments and this, in itself, would direct attention toward the stronger components where subsequent imaging would be expected to produce better topographical images. The biases used to observe various components could provide useful information about the surface interaction itself.

The observation of superconductivity[32,33] in electron-doped C_{60} compounds heightened the interest in this already well-studied molecule. Naturally, this interest has extended to STM, yielding many fascinating studies and images involving surface-adsorbed C_{60} molecules exposed to electron-rich doping agents.[9,29–31,34,35] Unfortunately, the doping agents (usually alkali metals because of their high electropositivity and volatility) do not show up in the resulting STM images and so their effect on the local site symmetry is uncertain. However, their presence on the surface could well be expected to perturb the MOs to an even greater extent than that caused by the surface alone, perhaps leading to complete loss of degeneracy.

Regardless of this, there is another reason to suspect that further degeneracy reduction may occur in surface-adsorbed doped C_{60}. As the surface-adsorbed molecule has, at most, doubly degenerate MOs, partial occupancy of an *E*-type orbital, as would occur if there was charge transfer to the fullerene atom, would result in a system liable to symmetry reduction as a consequence of electron-vibration interactions. Indeed, one of the most interesting claims surrounding this class of compounds is that they provide direct visual evidence for the occurrence of the JT effect.[9] Unfortunately, the actual amount of charge transfer that occurs on adsorption doesn't seem to be well quantified and depends on the surface involved. Also, the very nature of STM, insomuch as it involves measurement of electron transport through the system under study, could be expected to engender a transient JT effect in otherwise neutral C_{60}. Just such an argument has been recently used[1] to explain the form of "vibronic-like" sidebands in dI/dV data recorded from C_{60} adsorbed on top of a self-assembled molecular template (for isolation purposes) on Au(111).

The fact that charge transfer, counter ions and JT effects could have a substantial effect on the form of the resulting STM image have led us to focus the current paper on the simple, undoped C_{60}—surface system with no charge transfer. It is interesting, however, to consider what effects could, in principle, be observed in STM images as a result of splitting of the molecular orbitals due to the JT effects that will occur in charged fullerene ions. It is intended that a detailed investigation of this subject will form the basis of a subsequent paper. However, some preliminary results, concerned with the dynamical aspect of the problem as applied to $E \otimes e$ and $T \otimes h$ coupling regimes, including a discussion relating to charge transfer, may be found in Ref. 36.

As well as splitting molecular orbitals, another feature of the JT effect is that it will cause a geometric distortion of the C_{60} molecule. Other interactions could also cause geometric distortions. However, it is very unlikely that the intramolecular detail derived from individually imaged C_{60} molecules will be of sufficiently high resolution to resolve the small structural changes expected for these strongly bonded cage

molecules until there is a dramatic increase in device sensitivity. Thus we expect that ignoring geometric distortions is readily justifiable.

It is hoped that the images presented here may be a useful aid for identifying features observed via STM, and, perhaps, avoid misinterpretation of novel data. Of particular interest would be the observation of images which could be unequivocally assigned to HOMO, LUMO, or LUMO+1 origins. In this way, the pattern of surface-induced splitting can be put on a more quantitative footing and used to determine important information about the interactions responsible.

ACKNOWLEDGMENT

We gratefully acknowledge the support of EPSRC (U.K.) for funding this work (Grant No. EP/E030106/1).

*janette.dunn@nottingham.ac.uk; http://www.nottingham.ac.uk/~ppzjld

[1] T. Frederiksen, K. J. Franke, A. Arnau, G. Schulze, J. I. Pascual, and N. Lorente, Phys. Rev. B **78**, 233401 (2008).
[2] C. Silien, N. A. Pradhan, W. Ho, and P. A. Thiry, Phys. Rev. B **69**, 115434 (2004).
[3] J. G. Hou, Jinlong Yang, Haiqian Wang, Qunxiang Li, Changgan Zeng, Hai Lin, Wang Bing, D. M. Chen, and Qingshi Zhu, Phys. Rev. Lett. **83**, 3001 (1999).
[4] X. H. Lu, M. Grobis, K. H. Khoo, S. G. Louie, and M. F. Crommie, Phys. Rev. Lett. **90**, 096802 (2003).
[5] X. Lu, M. Grobis, K. H. Khoo, S. G. Louie, and M. F. Crommie, Phys. Rev. B **70**, 115418 (2004).
[6] H. I. Li *et al.*, Phys. Rev. Lett. **103**, 056101 (2009).
[7] T. Hashizume *et al.*, Phys. Rev. Lett. **71**, 2959 (1993).
[8] E. I. Altman and R. J. Colton, Phys. Rev. B **48**, 18244 (1993).
[9] A. Wachowiak, R. Yamachika, K. H. Khoo, Y. Wang, M. Grobis, D. H. Lee, S. G. Louie, and M. F. Crommie, Science **310**, 468 (2005).
[10] T. Hashizume, X. D. Wang, Y. Nishina, H. Shinohara, Y. Saito, Y. Kuk, and T. Sakurai, Jpn. J. Appl. Phys., Part 2 **31**, L880 (1992).
[11] Y. Deng and C. N. Yang, Phys. Lett. A **170**, 116 (1992).
[12] I. D. Hands, J. L. Dunn, C. A. Bates, and V. Z. Polinger, Chem. Phys. **278**, 41 (2002).
[13] E. Clementi and D. L. Raimondi, J. Chem. Phys. **38**, 2686 (1963).
[14] A. M. Bradshaw and N. V. Richardson, Pure Appl. Chem. **68**, 457 (1996).
[15] M. Casarin, D. Forrer, T. Orzali, M. Petukhov, M. Sambi, E. Tondello, and A. Vittadini, J. Phys. Chem. C **111**, 9365 (2007).
[16] S. Bhagavantam and D. Suryanarayana, Acta Crystallogr. **2**, 21 (1949).
[17] C. C. Chancey and M. C. M. O'Brien, *The Jahn-Teller Effect in* C_{60} *and Other Icosahedral Complexes* (Princeton University Press, Princeton, 1997).
[18] X. Cao and Y. Wang, Int. J. Quantum Chem. **77**, 615 (2000).
[19] J. Tersoff and D. R. Hamann, Phys. Rev. B **31**, 805 (1985).
[20] K. Aït-Mansour, P. Ruffieux, P. Gröning, R. Fasel, and O. Gröning, J. Phys. Chem. C **113**, 5292 (2009).
[21] M. Grobis, X. Lu, and M. F. Crommie, Phys. Rev. B **66**, 161408(R) (2002).
[22] H. Jensen, J. Kröger, N. Néel, and R. Berndt, Eur. Phys. J. D **45**, 465 (2007).
[23] K. Motai, T. Hashizume, H. Shinohara, Y. Saito, H. W. Pickering, Y. Nishina, and T. Sakurai, Jpn. J. Appl. Phys. **32**, L450 (1993).
[24] N. Néel, L. Limot, J. Kröger, and R. Berndt, Phys. Rev. B **77**, 125431 (2008).
[25] N. A. Pradhan, N. Liu, and W. Ho, J. Phys. Chem. B **109**, 8513 (2005).
[26] G. Schull and R. Berndt, Phys. Rev. Lett. **99**, 226105 (2007).
[27] J. I. Pascual, J. Gómez-Herrero, C. Rogero, A. M. Baró, D. Sánchez-Portal, E. Artacho, P. Ordejón, and J. M. Soler, seeing molecular orbitals, Chem. Phys. Lett. **321**, 78 (2000). Parts of Fig. 2 reprinted with permission from Elsevier, Copyright (2000).
[28] R. C. Haddon, L. E. Brus, and K. Raghavachari, Chem. Phys. Lett. **125**, 459 (1986).
[29] Y. Wang, R. Yamachika, A. Wachowiak, M. Grobis, and M. F. Crommie, Nature Mater. **7**, 194 (2008).
[30] Y. Wang, R. Yamachika, A. Wachowiak, M. Grobis, K. H. Khoo, D. H. Lee, S. G. Louie, and M. F. Crommie, Phys. Rev. Lett. **99**, 086402 (2007).
[31] K. Tsuchie, T. Nagao, and S. Hasegawa, Phys. Rev. B **60**, 11131 (1999).
[32] A. F. Hebard, M. J. Rosseinsky, R. C. Haddon, D. W. Murphy, S. H. Glarum, T. T. M. Palstra, A. P. Ramirez, and A. R. Kortan, Nature (London) **350**, 600 (1991).
[33] M. J. Rosseinsky, A. P. Ramirez, S. H. Glarum, D. W. Murphy, R. C. Haddon, A. F. Hebard, T. T. M. Palstra, A. R. Kortan, S. M. Zahurak, and A. V. Makhija, Phys. Rev. Lett. **66**, 2830 (1991).
[34] H. Hosoi, S. Nagashima, E. Hatta, K. Sueoka, and K. Mukasa, Jpn. J. Appl. Phys., Part 1 **38**, 5239 (1999).
[35] A. Tamai, A. P. Seitsonen, R. Fasel, Z. X. Shen, J. Osterwalder, and T. Greber, Phys. Rev. B **72**, 085421 (2005).
[36] I. D. Hands, J. L. Dunn, C. S. A. Rawlinson, and C. A. Bates, in *The Jahn-Teller Effect*, Springer Series in Chemical Physics Vol. 97, edited by H. Koeppel, D. R. Yarkony, and H. Barentzen (Springer-Verlag, Berlin, 2009), pp. 517–551.